Control Method of Flying Capacitor Converter Operated in Discontinuous Current Mode and Critical Current Mode

Jun-ichi Itoh, Ryoichi Ishibashi, Hoai Nam Le,
Nagisa Takaoka, Keisuke Kusaka
Dept. of Electrical, Electronics and Information Engineering
Nagaoka University of Technology
Nagaoka, Niigata, Japan
itoh@vos.nagaokaut.ac.jp

Katsutaka Tanabe
Omron Co., Ltd.
Kusatsu, Shiga, Japan
katsutaka_tanabe@omron.co.jp

***Abstract*— This paper proposes the control method of a three-level flying-capacitor converter (FCC), which is operated in discontinuous-current-mode (DCM) and critical current mode (CRM) to reduce the current ripple. An inverter connected to a single-phase grid requires a boost chopper and grid-connected inverter. In particular, reducing the volume of the boost inductor in the boost chopper is required. The DCM method is applied in order to minimize the volume of the boost inductor. However, the switching devices with high current rating are required due to a high current ripple when DCM is applied to a typical boost converter. In addition, FCC reduces the peak current of the boost inductor by the charging and discharging periods of the flying capacitor. In the proposed control method, FCC is designed to be operated in CRM at heavy load and DCM at light load. Due to the charging and discharging of the flying capacitor, the inductor current ripple in FCC is reduced compared to that of the typical boost converter with the same inductance. The validity of the proposed control method is confirmed with a 1-kW prototype. As a result, an efficiency of 96.2% is achieved at the 1-kW output power and the boost ratio of three.**

Keywords—Discontinuous Current Mode; Flying capacitor converter

I. INTRODUCTION

In recent years, photovoltaic power generation systems have attracted attention as renewable power sources [1-6]. In general, converter topologies for these systems consists of a boost circuit and a grid-tied inverter. High power density and high efficiency are required for these power converters. In particular, the boost inductor in the boost converter occupies a large volume in the system. Therefore, miniaturization of this boost inductor is strongly demanded [7].

One of the ideas to downsize the boost inductor is applying discontinuous current mode (DCM) to an inductor current control [8-11]. DCM reduces the inductor volume due to the required inductance in DCM is smaller than continuous current mode (CCM). However, the increased peak value of the current may increase conduction loss of switching devices and copper loss of the inductor. A large current ripple occurs as compared with CCM in the trade-off of a small inductor when DCM is applied to the boost converter. This high current ripple significantly increases the conduction loss in the switching devices, requiring a larger heat sink. Hence, the effect on the miniaturization of a system by the DCM operation in the boost converter is restricted.

As a method of reducing the peak current value, there is a three-level flying capacitor converter (FCC) to which DCM is applied [12]. Further inductor volume reduction is expected by combining the inductor volume reduction effect of DCM and the current ripple reduction effect of FCC [13]. In the literature [12], the boost inductor current waveform is controlled to be triangular. Thus, the effect of reducing the peak value of the current passing through the element is insufficient since the current peak value is more than twice the average current. Also, in the CCM operation, the flying capacitor voltage converges to approximately half of the output voltage without controlling. However flying capacitor voltage is not balanced in the DCM operation. The control method of the flying capacitor voltage has not been mentioned in the literature [12].

This paper proposes a DCM control method for a three-level FCC in order to increase the power density of a DC-DC converter. The proposed control operates FCC in four modes; two of which are same as these in the boost converter, whereas the other two modes are charging and discharging modes of the flying capacitor. Thus, this results in the operation of FCC with critical current mode (CRM) at heavy load and under DCM at light load. Due to the charge/discharge of the flying capacitor, the peak of the inductor current is reduced, resulting in the decrease in the conduction loss as well as the turn-off loss. The originality of this paper is the clarification of the duty-ratio calculation for FCC operated under DCM to achieve the current ripple. The proposed control method is tested in experimental results.

II. CIRCUIT CONFIGURATION

A. Three-level Fling Capacitor Converter

Figure 1 shows the FCC. The number of switching devices of the typical boost converter is two, whereas, the number of elements of FCC is four. Although the number of switching devices increases, the voltage which is applied to each switching device is half of that in the boost converter. Therefore, since devices with low on-resistance are used, it is possible to achieve the same conduction loss with the same RMS current. In this paper, DCM and CRM are applied to FCC in order to reduce the boost inductor current ripple, decreasing the RMS current value against average current value. Furthermore, since the required inductance value by applying DCM is reduced, it is possible to downsize the inductor. Therefore, both high efficiency and miniaturization are achieved with the proposed method.

B. Boost inductor current of each operation modes

Figure 2 shows the operation modes of FCC [14]. In the proposed method, the current i_L flowing through the inductor L is controlled using four modes; Mode I to VI. Details of each mode are described as following.

Mode I

In Mode I, energy is stored in L by turning on S_3 and S_4. The slope a_1 of the inductor current in this mode is expressed as

$$a_1 = \frac{v_{in}}{L} \quad (1),$$

where v_{in} is the input voltage, L is the inductance value of the boost inductor.

Mode II

In Mode II, by turning on S_2 and S_4, the energy is stored in C_{fc}. The slope a_2 of the inductor current in this mode is expressed as

$$a_2 = \frac{v_{in} - v_{fc}}{L} \quad (2),$$

where v_{fc} is the voltage of the flying capacitor $C_{fc.}$

Mode III

In Mode III, by turning on S_1 and S_3, the energy stored in C_{fc} and L is released to the output side v_{dc}. The slope a_3 of the inductor current in this mode is expressed as

$$a_3 = \frac{v_{in} - \left(v_{dc} - v_{fc}\right)}{L} \quad (3),$$

where v_{dc} is output voltage.

Mode IV

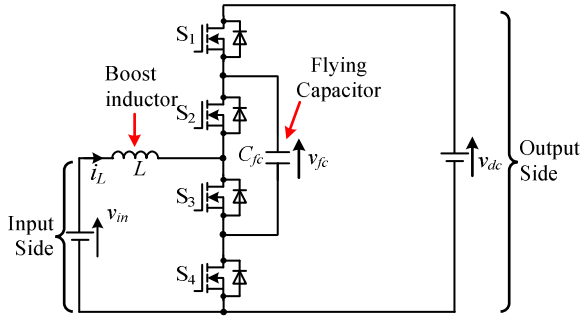

Fig. 1. Circuit diagram of three-level flying capacitor converter.

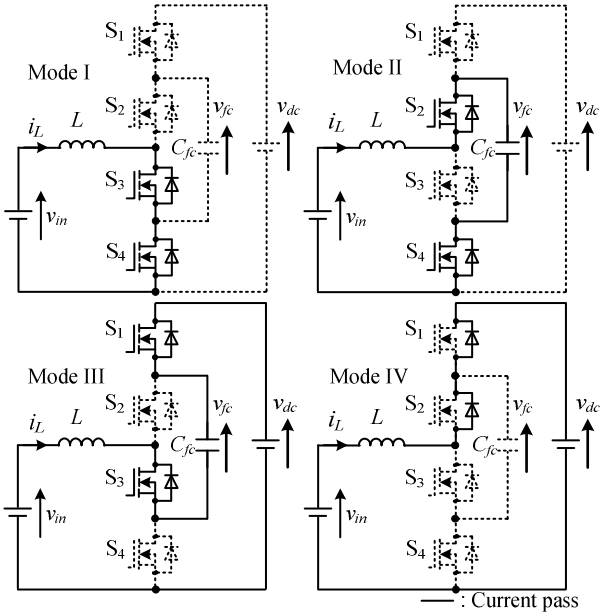

Fig. 2. Operation modes of flying capacitor converter.

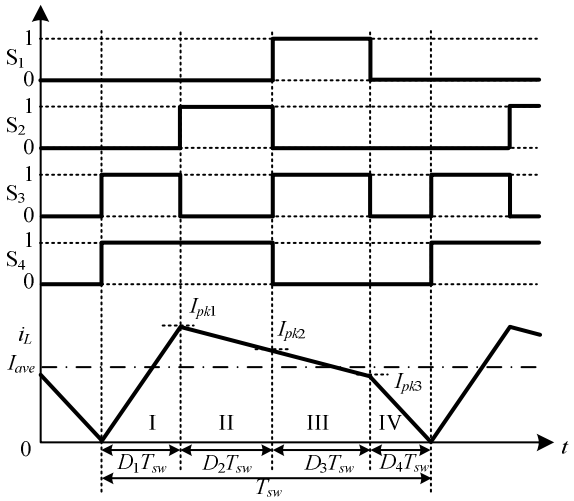

Fig. 3. Inductor current waveform and gate signals of MOSFETs of FCC in rated power.(rated load mode)

In Mode IV, by turning on S_1 and S_2, the energy stored in L is released to the output side. The slope a_4 of the inductor current in this mode is expressed as

$$a_4 = \frac{v_{in} - v_{dc}}{L} \quad (4).$$

Figure 3 shows the inductor current waveform in each switching mode during one switching cycle. This control method is obtained by adding Mode II and Mode III to the operation mode of the boost converter, which is composed of Mode I and Mode IV. Consequently, the inductor current i_L becomes a trapezoidal waveform. The current peak is reduced as compared with the boost converter when the same power is transmitted.

III. Derivation of Switching Duty Ratio

A. Heavy load region

In this section, a derivation method of the duty ratio of each mode is described. The duty ratio is determined so that the boost inductor current becomes CRM in heavy load. In this control, since there are four switching operation modes, it is necessary to obtain four switching duties. Here, the current peak values I_{pk1}, I_{pk2}, and I_{pk3} in the respective operation modes are expressed as

$$I_{pk1} = A_1 D_1 T_{sw} = \frac{v_{in}}{L} D_1 T_{sw} \quad (5),$$

$$I_{pk2} = A_2 D_2 T_{sw} + I_{pk1} = \frac{v_{in} - v_{fc}}{L} D_2 T_{sw} + I_{pk1} \quad (6),$$

$$I_{pk3} = A_4 D_4 T_{sw} = \frac{v_{in} - v_{dc}}{L} D_4 T_{sw} \quad (7),$$

where D_1, D_2, D_3, and D_4 are the duties in the respective operation modes in Fig. 3, T_{sw} is the switching period.

As FCC is operated under CRM at heavy load, the sum of the four duties is expressed as

$$D_1 + D_2 + D_3 + D_4 = 1 \quad (8).$$

Note that the operation of FCC under CRM at heavy load suppresses the increase in the current peak compared to DCM.

The flying capacitor voltage v_{fc} is a half value of the output voltage v_{dc}, and the ratio of the input voltage to the output voltage is assumed to be 2 or more. The slope a_2 and a_3 in (2) and (3) are equal.

The sum of the average power in each switching mode equals to the transmission power, which is expressed as

$$\frac{1}{2} I_{pk1} D_1 T_{sw} + \frac{1}{2}\left(I_{pk1} + I_{pk3}\right)\left(1 - D_1 - D_4\right) T_{sw} + \frac{1}{2} I_{pk3} D_4 T_{sw} = I_{ave} T_{sw} \quad (9).$$

From (10) and (11), D_1 and D_4 are represented as

$$D_4 = \frac{v_{in} - \sqrt{-v_{in}^{\,2} + v_{in} v_{dc} - 2 I_{ave} L f_{sw} v_{dc}}}{v_{dc}} \quad (10),$$

$$D_1 = -\frac{2 v_{in}}{v_{dc}} + 1 + D_4 \quad (11).$$

In FCC, in order to keep the voltage of C_{fc} constant, the time product of the current flowing through C_{fc} must be controlled to be zero during one switching period. Therefore, the duties are designed so that the current time products of i_L in Mode II and Mode III are equal, expressing as

$$\frac{1}{2}\left(I_{pk1} + I_{pk2}\right) D_2 T_{sw} - \frac{1}{2}\left(I_{pk2} + I_{pk3}\right) D_3 T_{sw} = 0 \quad (12).$$

From (14), (15), D_4 and D_1 are represented as

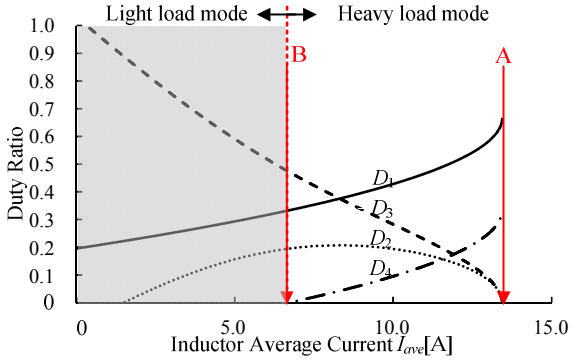

Fig. 4. Relationship between average current and duty. (Heavy load mode)

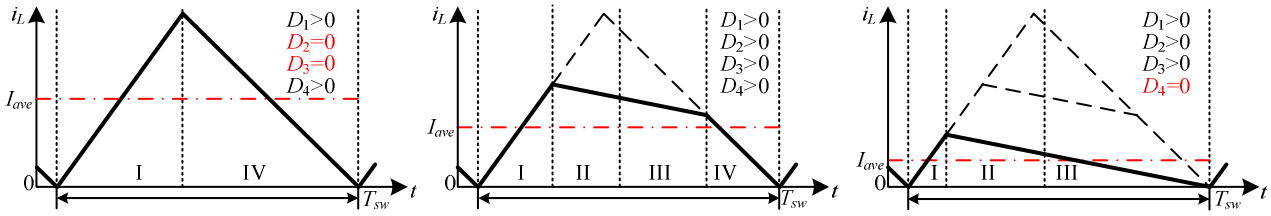

(a)Maximum power (condition A of Fig. 4) (b)Midium power (c)Minimum power(condition B of Fig. 4)

Fig. 5. Transition of current waveform according to load

$$D_2 = \frac{-B + \sqrt{B^2 - 4AC}}{2A} \quad (13),$$

$$D_3 = D_{23} - D_2 \quad (14),$$

where

$$\begin{cases} D_{23} = 1 - D_1 - D_4 \\ A = 2\left(v_{in} - \dfrac{v_{dc}}{2}\right) \\ B = 3v_{in}D_1 - \left(v_{in} - \dfrac{v_{dc}}{2}\right)D_{23} - \left(v_{in} - v_{dc}\right)D_4 \\ C = \left\{-v_{in}D_1 + \left(v_{in} - v_{dc}\right)D_4\right\}D_{23} \end{cases} \quad (15).$$

Figures 4–5 shows the relationship among the duties and the boost inductor average current and the current waveform variation of each load when the voltage condition and circuit parameters are as an example. As can be seen in Fig. 4, input average current I_{ave} has an upper limit and a lower limit because all of the duty must be taken only positive. This is because the slope of the current waveform depends on the voltage conditions and the circuit parameters as shown in Fig. 5 (a) and (c). Therefore, this strategy is applied only in heavy load region.

B. Light load mode

In this section, the operation mode for a light load is described. This control method is obtained by adding the zero current period after Mode III. The derivation method of the duty for the light load is described below.

Figure 6 shows the inductor current waveform in each switching mode during one switching cycle. Here, the current peak values I_{pk1} and I_{pk2} in the respective operation modes are expressed as (5‑6). From the previous section, the slope a_2 equals to a_3 due to the flying capacitor voltage v_{fc} is half of output voltage v_{dc}. From this relationship, D_{23} that is sum of Mode II and Mode III period expressed as

$$D_{23} = D_2 + D_3 = \frac{2v_{in}}{v_{dc} - 2v_{in}} D_1 \quad (16).$$

The sum of the average power in each switching mode equals to the transmission power, which is expressed as

$$\frac{1}{2} I_{pk1} D_1 T_{sw} + \frac{1}{2} I_{pk1} D_{23} T_{sw} = I_{ave} T_{sw} \quad (17).$$

From (5), (6), (16) and (17), D_1 is represented as

$$D_1 = \sqrt{2LI_{ave} f_{sw} \frac{v_{dc} - 2v_{in}}{v_{in} v_{dc}}} \quad (18).$$

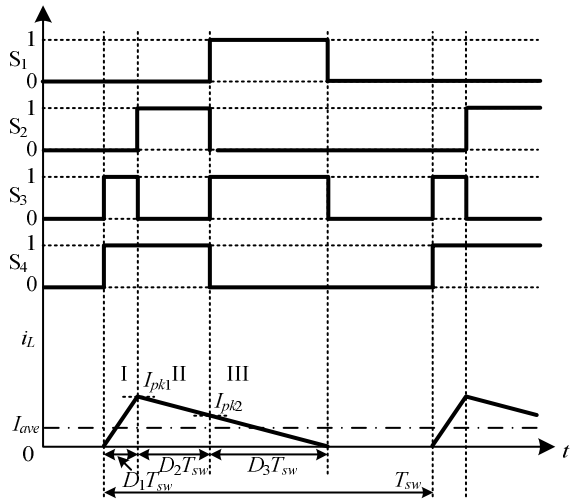

Fig. 6. Inductor current waveform and gate signals of MOSFETs of FCC in rated power.(rated load mode)

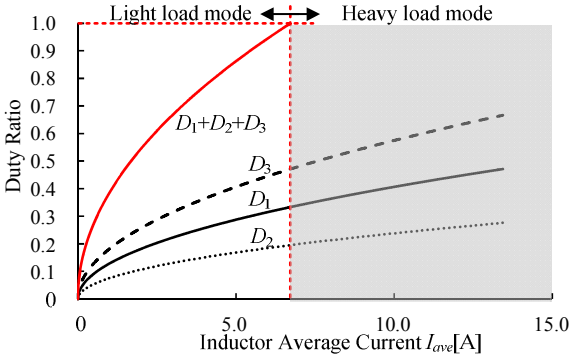

Fig. 7. Relationship between average current and duty. (light load mode)

In FCC, in order to keep the voltage of C_{fc} constant, the time product of the current flowing through C_{fc} must be controlled to be zero during one switching period. Therefore, the duties are designed so that the current time products of i_L in Mode II and Mode III are equal, expressing as (12). Substituting (5) and (6) for (12), D_3 and D_2 is expressed as

$$D_3 = \frac{v_{in}\sqrt{2}}{v_{dc} - 2v_{in}} D_1 \quad (19),$$

$$D_2 = D_{23} - D_3 \quad (20).$$

Figure 7 shows the relationship among the duties and the inductor average current when the voltage condition and circuit parameters are the same as in the previous section. As can been seen in Fig. 7, since the sum of the duties is possible to take less than 1, it is confirmed that there are an upper limit value for the value that the average current I_{ave} is possible to generate.

IV. Fling Capacitor Voltage Control

Figure 8 shows the flying capacitor voltage waveform in each switching mode during one switching cycle. In the previous section, the duty ratio is derived under the assumption of that the

flying capacitor C_{fc} voltage v_{fc} is kept at half of the DC-link voltage. However, the voltage of flying capacitor varies since Mode II and Mode III charge and discharge the flying capacitor. Furthermore, the inductance information of the boost inductor is required in calculating the duty ratio, but the actual inductance value varies depending on current and heat. Therefore, the flying capacitor voltage may diverge since an error occurs in the duty calculation. Also, (12) does not satisfy. Therefore, in this paper, feedback control is introduced to the flying capacitor voltage.

Figure 9 shows the block diagram of the boost inductor current control and the flying capacitor voltage control system. First, the original duty ratio is calculated based on the parameters such as the average inductor current command I_{ave}^* and the input and output voltage. Next, the time ratio of Mode II, III is adjusted by the compensation duty generated by the proportional controller. A voltage command of 1p.u. is inputted as the command value for P control. Here, 1p.u. is defined as the half-value of the output voltage. In this control, increase the ratio of Mode II (flying capacitor charging mode) when the flying capacitor voltage v_{fc} decreases. On the other hand, increase the ratio of Mode III (flying capacitor discharging mode) when the flying capacitor voltage v_{fc} increases. Thus, the flying capacitor voltage is kept by the control even when the parameter variation of the circuit occurs.

V. Simulation and Experimental Results

A. Heavy load

In this section, the fundamental operation of the FCC applying the proposed DCM is verified by the prototype.

Table 1 shows the circuit parameters. In this paper, assuming that a 200 V single phase grid-tied inverter is connected, the output voltage is set to 300 V. In addition, the rated power is 1 kW (1p.u.)

Figure 10 shows a comparison of the peak inductor current i_L between the boost converter operated with DCM and FCC operated with CRM under the same conditions of the boost inductance value and the switching frequency. Fig. 10 confirms that FCC with proposed control reduces inductor current peak by 21% compared to that of the boost chopper operated with DCM.

Figure 11 shows the operating waveforms when the current command is 0.8 p.u. and 1 p.u. From Fig. 11, it is confirmed that the boost inductor current i_L is controlled in a trapezoidal waveform. The average power at this time was 0.68 p.u. and 0.88 p.u., respectively. This is because the average current is controlled by an open loop, so it is affected by dead time and voltage fluctuation of the flying capacitor.

Figure 12 shows operating waveforms when the power command is changed stepwise from 0.8p.u. to 1p.u., and vice versa. As can be seen from Fig. 12, the flying capacitor voltage is controlled constant despite the load power fluctuation.

Figure 13 shows the operating waveform when the flying capacitor voltage command is step changed between 0.8p.u. and 1p.u. It is confirmed from Fig. 10 that the flying capacitor voltage follows the command and that the flying capacitor voltage is be controlled to a desired value by adjusting the

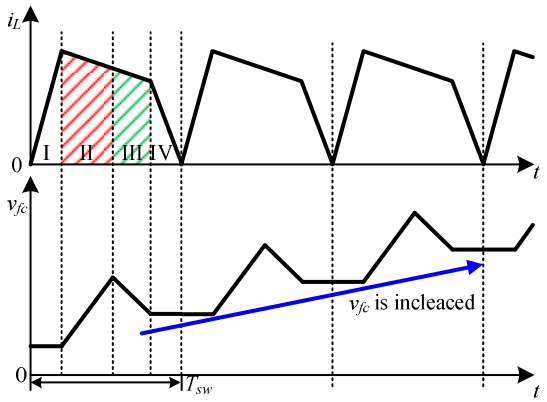

Fig. 8. Flying capacitor voltage change during Mode II and Mode III

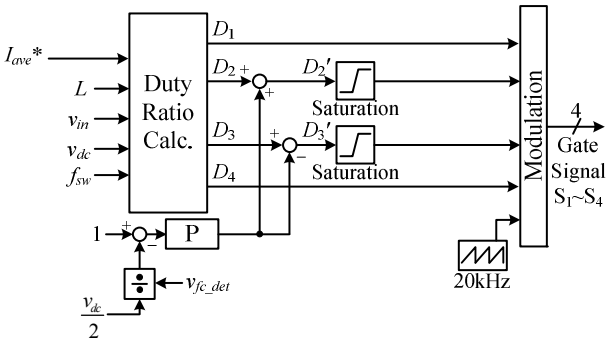

Fig. 9. Circuit diagram of flying capacitor converter.

TABLE I. Simration and Experimental Condition

Input voltage	v_{in}	100 V
Output voltage	v_{dc}	300 V
Switching frequency	f_{sw}	20 kHz
Boost inductor	L	124 μH
Flying Capacitor	C_{fc}	60 μF, 200 V *3 Parallel
Switching Devices	S_1-S_4	IXFN132N50P3
Gate Resistor		4.7 Ω

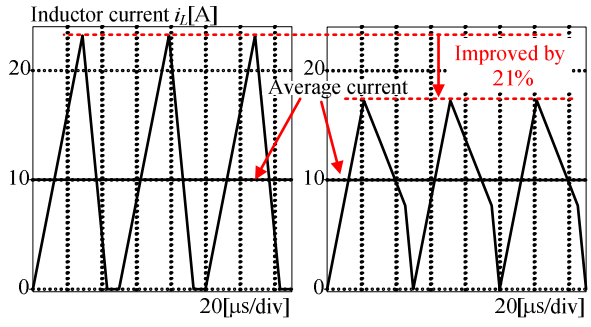

(a) Boost chopper in DCM. (b) FCC in CRM.

Fig. 10. Comparison of operation waveforms in simulation (I_{ave}=10 A).

switching duty ratio. As shown in Fig. 13 (a), when the flying capacitor voltage control is in the transient state, the inductor

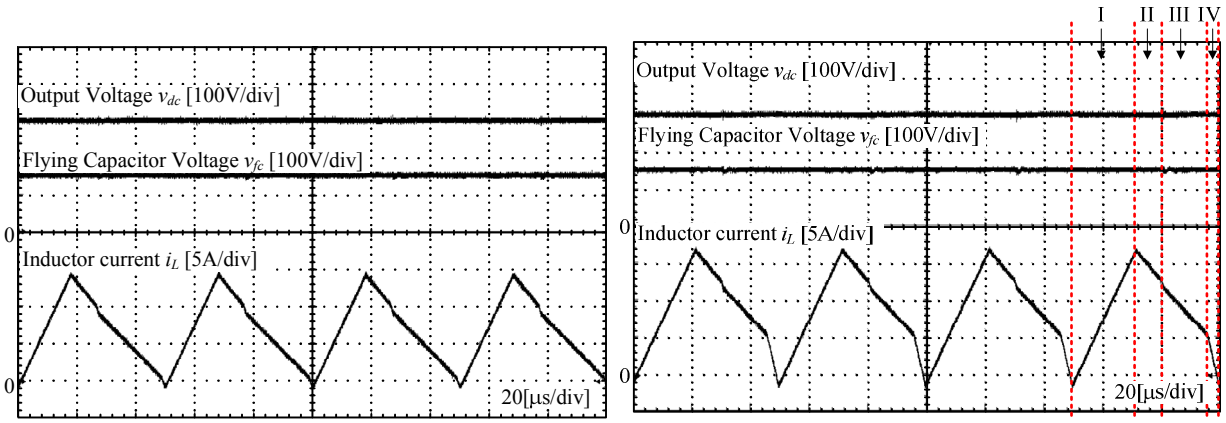

(a) I_{ave}^*=8 A (0.8 p.u.) (b) I_{ave}^*=10 A (1 p.u.)

Fig. 11. Operation waveforms of around current

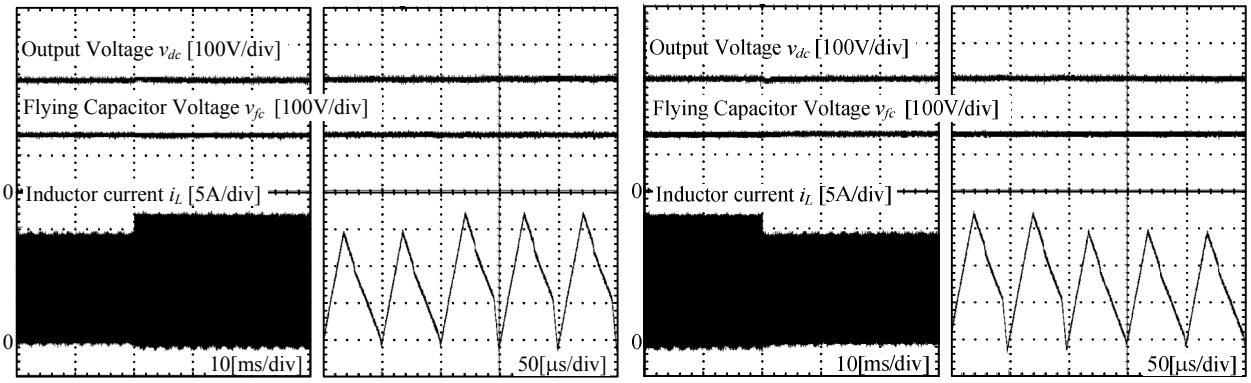

(a) Step up response (b) Step down response

Fig. 12. Experimental result for current step up response.(0.8 p.u. to 1 p.u.).

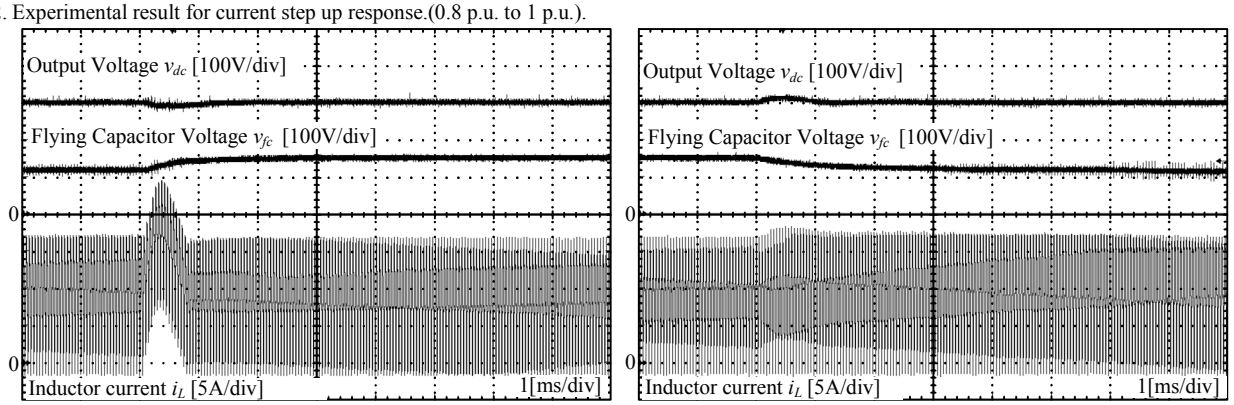

(a) Step up response. (0.8 p.u. to 1 p.u.) (b) Step down response. (1 p.u. to 0.8 p.u.)

Fig. 13. Experimental result for response of flying capacitor voltage.

current temporarily becomes CCM. This is because the current control is an open loop and the duty ratio of Mode I and Mode IV according to the fluctuation of the flying capacitor voltage is not adjusted.

Figure 14 shows the operating waveforms when the current command is 0.2p.u. and 0.6p.u. From Fig. 14, it is confirmed that the boost inductor current i_L is controlled in a triangular waveform. The average power at this time is 0.17p.u. and 0.53p.u., respectively. This is because the average current is controlled by an open loop, so it is affected by dead time and voltage fluctuation of the flying capacitor. Application of feedback control for boost inductor current is a future subject.

Figure 15 shows the efficiency characteristics. As the result, the maximum efficiency of 96.6% is achieved at 100 V of input voltage. This is cause that the input voltage is changed while the output voltage is constant. From the results, efficiency is decreased at heavy load and light load. At light load and heavy load, the boost inductor current approach triangular waveform due to duty calcration. Therefore, the current RMS value against average value is increase.

VI. Conclusions

This paper proposed the control method of FCC operated under CRM and DCM in order to reduce the current ripple. The proposed operation is verified by the prototype. The proposed

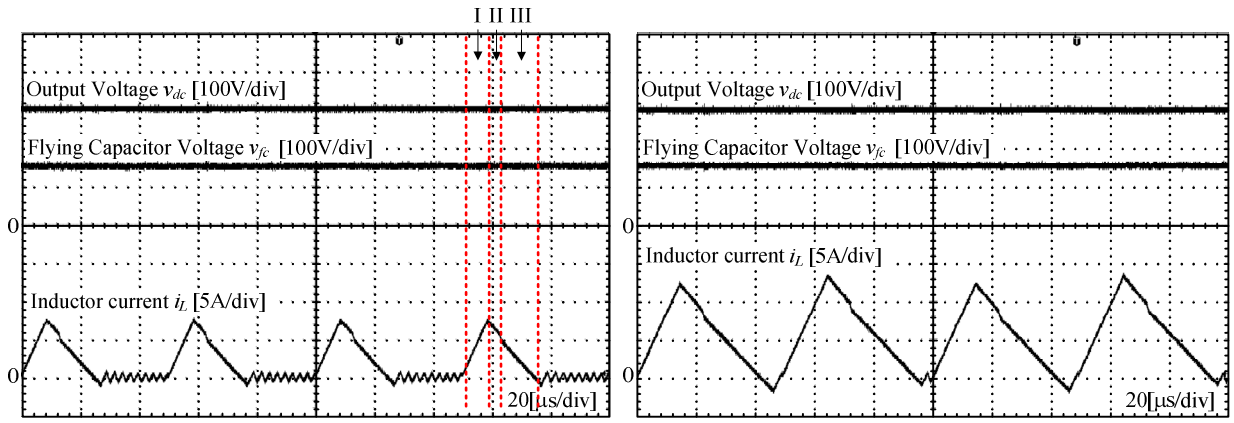

(a) I_{ave}^*=2 A (0.2 p.u.) (b) I_{ave}^*=6 A (0.6 p.u.)

Fig. 14. Experimental result for current step up response.

method is characterized by combining four switching modes and setting the inductor current waveform to trapezoidal wave shape so that it is possible to suppress the inductor current peak value and control the flying capacitor voltage at the same time. By applying the proposed method for boost inductor control of FCC, the boost inductor current is controlled in a trapezoidal waveform and the flying capacitor voltage is controlled by adjusting the duty ratio of Mode II and Mode III. The experimental results show relevance of this method. In experimental results, the maximum efficiency of 96.6% is achieved at 100 V of input voltage. And an efficiency of 96.2% is achieved at the 1-kW output power and the boost ratio of three.

In the future, we are planning to introduce current feedback control, analyze losses.

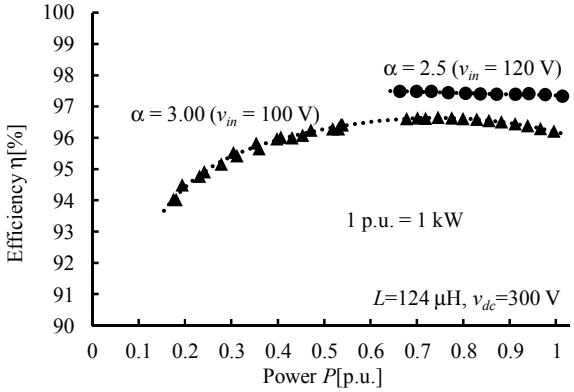

Fig. 15. Efficiency characteristic.

REFERENCES

[1] Yi Tang, Wenli Yao, Poh Chiang Loh, Frede Blaabjerg : "Highly Reliable Transformers Photovoltaic Inverters With Leakage Current and Pulsating Power Elimination", IEEE Trans. on Industrial Electronics, Vol. 63, No. 2, pp. 1016-1026 (2016)

[2] T. Shimizu, K. Wada, N. Nakamura : "Flyback-Type Single-Phase Utility Interactive Inverter With Power Pulsation Decoupling on the DC Input for an AC Photovoltaic Module System", IEEE Trans. on Power Electronics, Vol. 21, No. 5, pp. 1264-1272 (2006)

[3] Jinsoo Han, Jin-Doo Jeong, Ilwoo Lee, Sang-Ha Kim : "Low-cost monitoring of photovoltaic systems at panel level in residential homes based on power line communication" IEEE Trans. on Consumer Electronics, Vol. 63, No. 4, pp. 435-441 (2017)

[4] Toshihisa Shimizu, Keiji Wada and Naoki Nakamura : "Flyback-Type Single-Phase Utility Interactive Inverter With Power Pulsation Decoupling on the DC Input for an AC Photovoltaic Module System", IEEE Transactions on Power Electronics, Vol. 21, No. 5, pp.1264-1272 (2006)

[5] Subhendu Dutta, Kishore Chatterjee : "A Buck and Boost Based Grid Connected PV Inverter Maximizing Power Yield From Two PV Arrays in Mismatched Environmental Conditions", IEEE Transactions on Industrial Electronics, Vol. 65, No. 7 (2018)

[6] Yuxiang Shi, Ren Xie, Lu Wang, Yanjun Shi and Hui Li : "Switching Characterization and Short-Circuit Protection of 1200 V SiC MOSFET T-Type Module in PV Inverter Application", IEEE Transactions on Industrial Electronics, Vol. 64, No. 11, pp.9135-9143 (2017)

[7] Jun Imaoka, Kenkichiro Okamoto, Shota Kimura,Mostafa Noah, Wilmar Martinez, Masayoshi Yamamoto, Masahito Shoyama, : "A Magnetic Design Method Considering DC-Biased Magnetization for Integrated Magnetic Components Used in Multiphase Boost Converters", IEEE Trans. on Power Electronics, Vol. 33, No. 4, pp. 3346-3362 (2018)

[8] H. N. Le, K. Orikawa, J. Itoh : "DCM Control Method of Boost Converter based on Conventional CCM Control", The 2014 International Power Electronics Conference, No. 21A4-5, pp. 3661-3666 (2014)

[9] Hoai Nam Le, Daisuke Sato, Koji Orikawa, Jun-ichi Itoh : "Efficiency Improvement at Light Load in Bidirectional DC-DC Converter by Utilizing Discontinuous Current Mode", 17th Conference on Power Electronics and Applications, EPE'15-ECCE Europe, No. DS1b-Topic 3-0484, (2015)

[10] Mahdi Salimi, Abel Zakipour, "Direct Voltage Regulation of DC–DC Buck Converter in a Wide Rangeof Operation using Adaptive Input-Output Linearization" IEE of Japan Trans. on Electrical and Electronic Engineering, Vol. 10, pp. 85-91 (2015)

[11] Yasuhiro Sugimoto, Toru Sai, Kei Watanabe, Mikio Abe : "Feedback Loop Analysis and Optimized Compensation Slope of the Current-Mode Buck DC-DC Converter in DCM", IEEE Trans. on Circuits and Systems, Vol. 62, No. 1, p.311-319 (2015)

[12] Yiwei Tan, Chi-Seng Lam, Sai-Weng Sin, Man-Chung Wong, Rui Paulo Martins: "Design and Control of An Integrated 3-Level Boost Converter under DCM Operation", 2018 IEEE International Symposium on Circuits and Systems, pp. 1-5 (2018)

[13] J. Itoh, K. Matsuura, K. Orikawa: "Reduction of a Boost Inductance using a Switched Capacitor DC-DC Converter", ICPE 2011 - ECCE Asia, pp. 1315-1322 (2011)

[14] J. Itoh, K. Matsuura, K. Orikawa: "Reduction of a Boost Inductance using a Switched Capacitor DC-DC Converter", ICPE 2011 - ECCE Asia, pp. 1315-1322 (2011)